Effects of turbulence-induced colored noise on thermoacoustic instabilities in combustion chambers

Giacomo Bonciolini, Edouard Boujo and Nicolas Noiray

CAPS Laboratory, MAVT department ETH Zürich, 8092, Zürich, Switzerland

Abstract

Practical combustion systems are prone to thermoacoustic instabilities, which affect the mechanical integrity of the components. This paper investigates how the turbulence-induced-noise stochastically drives these thermoacoustic limit-cycles. A model of the constructive feedback between the flames and the combustor acoustics is proposed and includes a non-coherent forcing with finite correlation time. It constitutes a more accurate description of the non-linear stochastic dynamics observed in practical combustors, compared to the usual white-noise-forcing assumption. The outcome of this study consolidates the recent model-based output-only system identification methods, proposed by Noiray and Schuermans [1] to extract the governing parameters of the thermoacoustic dynamics.

Keywords: Combustion noise, colored noise, Van der Pol oscillator, system identification, time series analysis

1. Introduction

In the gas turbines research field, thermoacoustic instabilities in combustion chambers constitute one of the most difficult problem to address. The race for more efficient, less pollutant and more fuel and operational flexible systems is ongoing, towed by customers needs and environmental regulations [2]. The mechanisms ruling the physics of these instabilities are complex and their occurrence at a given engine operating point is difficult to predict.

In this context, the development of reliable combustion dynamics models is of primary importance. Considering that full scale turbulent-reactive-compressible Large-Eddy-Simulations require prohibitive numerical costs, the predictive tools under development are based on low-order network model for the treatment of the acoustics, complemented by experimentally measured data and computationally-cheaper numerical simulations [4, 5, 6, 7].

In parallel to this predictive-tools development effort, robust model-based system identification (SI) methods must be established in order to validate the aforementioned thermoacoustic network models. Indeed, these output-only SI strategies can be applied to real data in order to extract linear

This is a pre-print version. Presented at *International Symposium: Thermoacoustic Instabilities in Gas Turbines and Rocket Engines,* May 30 - June 02, 2016 Munich, Germany.

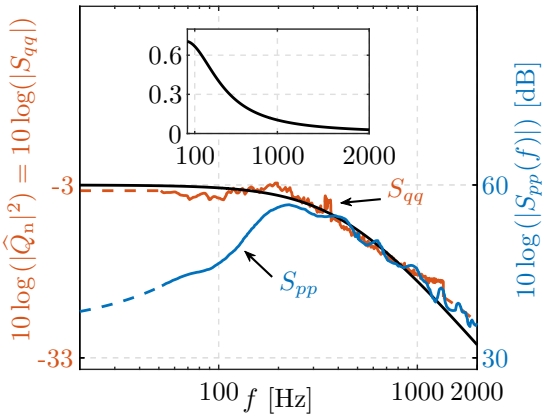

Figure 1: Example of turbulence induced heat release fluctuation $\widehat{Q}_\mathrm{n}$ (red, S_{qq}) and combustion noise (blue, S_{pp}) power spectra of an open flame radiating sound in the free field (adapted from reference [3]). The black line corresponds to an Ornstein-Uhlenbeck process, approximating S_{qq}. In the inset, the same Ornstein-Uhlenbeck noise with linear scales.

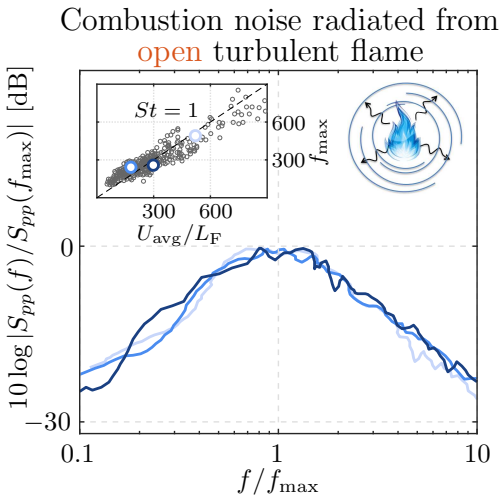

Figure 2: Example of normalized combustion noise spectra measured for different open flames configurations (adapted from reference [3]). In the inset, the frequency of the spectrum maximum is given as a function of the flow characteristics for a large set of operating conditions.

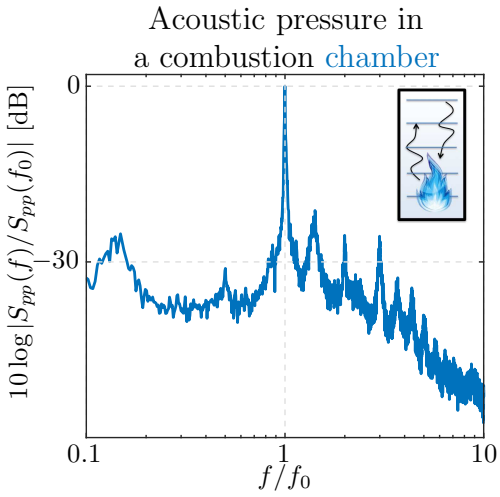

Figure 3: Typical acoustic pressure spectrum in a combustion chamber.

This is a pre-print version. Presented at *International Symposium: Thermoacoustic Instabilities in Gas Turbines and Rocket Engines,* May 30 - June 02, 2016 Munich, Germany.

growth rates hidden behind the nonlinear stochastic dynamics, and subsequently, to compare them with the ones predicted using thermoacoustic network models. System parameter identification is also of primary importance for the design of passive damping systems.
For the combustor physics description, one has to to simplify as much as possible the model while making sure that the governing mechanisms are included. Indeed, the more the number of parameters to identify is, the less the identification will be robust.
In practical systems, thermoacoustic limit cycles are driven by a stochastic forcing resulting from the intense turbulence in the combustor. Despite the fact that this forcing has a finite correlation time, it is often assumed that this noise is white. In this paper, the reliability of this assumption is investigated by comparing the dynamics and the statistics of white and colored noise driven self-sustained oscillators. The objective is to check whether the actual stochastic non-linear dynamics can be captured or not using a white noise forcing assumption. The potential consequences of that noise color on output only system identification methods are discussed, to understand if that can bias the results in practical cases, if not taken into account.

The thermoacoustic instabilities in turbulent combustion chambers can be modelled as a set of coupled stochastic differential equations, each describing the dynamics of one of the many thermoacoustic eigenmodes established in the combustor (e.g. [8]). The acoustic pressure at a given location can be approximated by the sum of their contribution: $p(x,t) = \sum_{i=1}^{\infty} \eta_i(t)\psi_i(x)$, where η_i denotes the amplitude of the i^{th} mode and ψ_i the spatial distribution of the corresponding natural acoustic mode of the chamber. It is possible to express the modal amplitude dynamics as a set of nonlinearly coupled stochastic oscillators (see [9]):

$$\ddot{\eta}_i(t) + \omega_i^2 \eta_i(t) = f_i(\eta_k, \dot{\eta}_k, ...) + \xi_i(t) \quad i,k = 1,..,m, \tag{1}$$

where $\omega_i = 2\pi f_i$ is the pulsation of the i^{th} natural acoustic mode and f is the non-linear function combining the effect of heat release fluctuation q and the chamber acoustic damping.
In eq. (1), $\xi_i(t)$ is the aforementioned additive stochastic forcing, resulting from the weighting by ψ_i of turbulence-induced non-coherent heat release rate fluctuation, having spectrum $\widehat{Q}_{\mathrm{n}}(\omega)$. An example of the correspondent power spectral density $S_{qq} = |\widehat{Q}_{\mathrm{n}}(\omega)|^2$ is plotted in fig. 1.
Considering ξ as a delta correlated forcing simplifies the modeling approach and has been used in most of the studies dealing with stochastically forced thermoacoustic limit cycles.
However, the actual power spectrum S_{qq} of the source therm $\widehat{Q}_{\mathrm{n}}$ is not constant, but it presents a characteristic low-pass filter behavior [3] (fig. 1, in red). The "color" of this noise forcing is due to a non-vanishing, although small, correlation time.
In case of an open turbulent flame placed in an unbounded environment, the radiated sound constitutes the so-called combustion noise [10]. Figure 1 shows the power spectra of both the source term $\widehat{Q}_{\mathrm{n}}$ (S_{qq}) and of the combustion noise radiated from an open turbulent flame (S_{pp}). One has to notice the bandpass characteristic of combustion noise spectrum, featuring a maximum in $f = f_{\max}$, in contrast with the low-pass one of $\widehat{Q}_{\mathrm{n}}$, having $f_{\max}$ as cut-off frequency. $\widehat{Q}_{\mathrm{n}}$ is there-

This is a pre-print version. Presented at *International Symposium: Thermoacoustic Instabilities in Gas Turbines and Rocket Engines,* May 30 - June 02, 2016 Munich, Germany.

fore a compact monopolar source, generating an acoustic pressure having a power law $P \propto f^2$ for $f < f_{\max}$. It is shown in the examples taken from [3] that the normalized combustion noise power spectra collapse on top of each others, indicating a general scaling law not depending on the flame characteristics (fig. 2).
In case of an enclosed thermoacoustic system, the situation is different. As an example, a typical acoustic pressure spectrum recorded in a combustion chamber, which is operated at a condition characterised by a strong thermoacoustic limit cycle, is presented in fig 3. As is often the case, a single mode dominates the spectrum, with a sharp peak of frequency f_0.
If one wants to perform non-linear system identification using a single mode description [1], one has to remove the effect of neighbouring thermoacoustic modes from the raw time traces. This can be done by bandpass filtering the data or by performing a modal projection if several simultaneous records at different location in the chamber are available. These data manipulations can, however, change the outcomes of output-only system identification methods, as the examined signal and its statistics can be sensibly altered. Therefore, the choice of the processing parameters, such as the filter bandwidth in case of filtering, has to be taken with care.
In the band around the considered mode natural frequency, S_{qq} is expected not to change significantly. Therefore, in this case, the use of a white noise approximation seems legitimate. This paper aims at bringing new insights in the effect of noise color on the system dynamics, and at addressing the question of the necessity to adopt or not this more refined model.
The outline of the present study is the following. In section 2, the theoretical background is covered, and an analytical model for colored noise is derived. In section 3, the white noise approximation is compared to the colored noise modelling of non-coherent heat release fluctuation, closer to reality. The aim is to investigate if, and under which circumstances, one can observe a substantial difference between the two models. Then, the effect of experimental data filtering, in the context of system identification, is addressed, in order to appreciate the errors that this practice could lead, if not properly performed.

2. Model of the system

The theoretical model of a colored noise driven self-sustained oscillator is presented in this section. This is supposed to mimic, in a simplified way, the main aspects of the real system dynamics. One of these, to fulfil the main purpose of this work, is the effect of turbulence-induced noise color. In section 2.1 the difference between noise radiated by open turbulent flames and the one recorded inside a combustion chamber is discussed. Then a model of colored noise is introduced in section 2.2. In section 2.3, the Van der Pol oscillator driven by white or colored noise is presented, and the probability density function for its oscillation amplitude is then derived.

This is a pre-print version. Presented at *International Symposium: Thermoacoustic Instabilities in Gas Turbines and Rocket Engines,* May 30 - June 02, 2016 Munich, Germany.

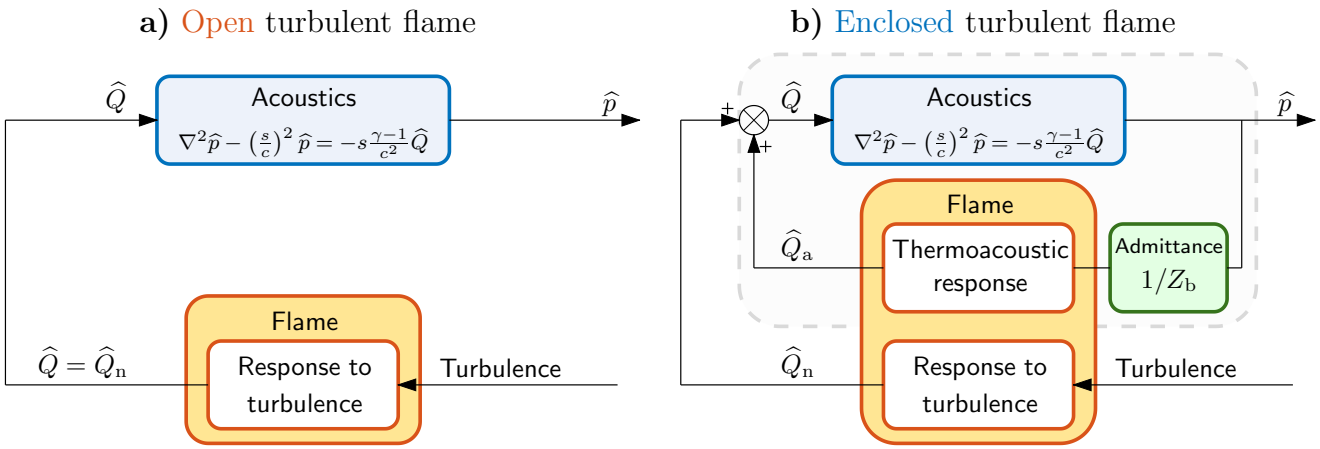

Figure 4: Network models for thermoacoustic systems. The open loop configuration (a) represents the case of open flames radiating noise in the free field. When the flame is bounded, a feedback system is generated (b). Here the acoustic block is fed by the total heat release fluctuation $\widehat{Q} = \widehat{Q}_\mathrm{a} + \widehat{Q}_\mathrm{n}$, and generates pressure fluctuations. These coherent perturbations act on the flame, that responds with $\widehat{Q}_\mathrm{a}$. The flame is also excited by incoherent forcing, due to the turbulence in the flow, that produces $\widehat{Q}_\mathrm{n}$. The closed system can be seen as well as a SISO one (grey shading): the external forcing is given by the incoherent component only, while the coherent response is a feedback that modifies the poles of the system (see also fig. 6c).

2.1. Theoretical background

The pressure fluctuation in the acoustic domain can be estimated making use of the Helmholtz equation and appropriate boundary conditions:

$$\nabla^2\widehat{p}(s,x) - \left(\frac{s}{c}\right)^2 \widehat{p}(s,x) = -s\frac{\gamma-1}{c^2}\widehat{Q}(s,x) \text{ in the domain,} \tag{2}$$

$$\frac{\widehat{p}(s,x)}{\widehat{u}(s,x)\cdot n} = Z(s,x) \quad \text{on boundaries,} \tag{3}$$

where $\widehat{p}$ and $\widehat{u}$ are the acoustic pressure and velocity fluctuations, s the Laplace variable, x the position, c the local speed of sound, γ the specific heat ratio, $\widehat{Q}$ the heat release fluctuation, n the outward normal to the boundary and Z the acoustic impedance. This equation stands if the Mach number is low.

Therefore, heat release fluctuations $\widehat{Q}$ from the flame constitute a source term for the acoustic pressure fluctuations $\widehat{p}$. If the flame is placed in an open environment, waves generated by the reaction zone are radiated away without reflections. An example of the spectral content of such sound field, i.e. the combustion noise [10], is given in fig. 2. $\widehat{Q}$, in this case, consists only in the turbulence induced noise-like fluctuation $\widehat{Q}_\mathrm{n}$ (see fig. 4a). In [11], a model for this mechanism is provided, linking turbulence to heat release fluctuation and then to sound radiation.

When the flame is placed within a container, e.g. into a combustion chamber, the acoustic field changes completely. In fact, as a consequence of the reflections at the boundaries, a series of natural acoustic modes is established in the domain. Any kind of source acting in the chamber excites

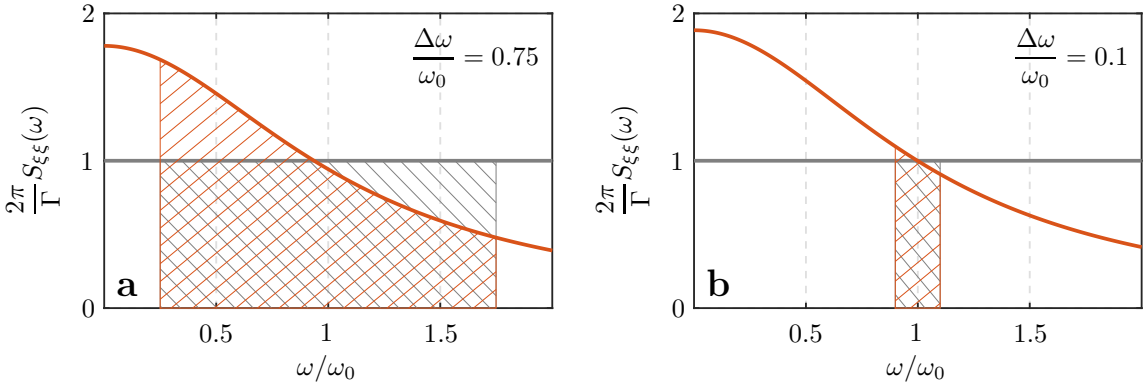

Figure 5: Comparison between white noise (grey) and colored noise (red) power spectra, normalised by the white noise intensity, for different iso-power bandwidths $\Delta\omega$. The power provided by the two types of noise is equal in the considered band (same area under the curve: note the linear scale). Note that $S_{\xi\xi}(\omega_0) \neq \Gamma/2\pi$. The same bands are afterwards used in fig. 9.

these modes in a way that depends on its distribution with respect to the modes shape. As result, for example, any mode having a node close to the source location is not excited. Therefore, the resulting acoustic field, is a superimposition of each mode response to the sources forcing. If the source consists, as in this case, in a flame, another peculiar aspect has to be considered. In fact, the induced heat release fluctuation $\widehat{Q}$ depends in this case on the local acoustic field. Therefore, the source depends on the sound field it generates, or equivalently, a feedback loop is created (see fig. 4b). This last fact can cause the instability of the thermoacoustic system, if heat release and pressure fluctuations interact constructively as exemplified by the dominant peak in (fig. 3).
However the flame, is also influenced by local hydrodynamic turbulent flow. The resulting heat release fluctuation is the aforementioned $\widehat{Q}_\mathrm{n}$. The turbulence-induced flow perturbations exhibits a much smaller spatial correlation than the acoustic ones, which are correlated over the entire combustor. This does not prevent it to be weighted as well on the modes shape: as discussed in the introduction and highlighted in eq. (1), what enters the mode amplitude equation is $\xi(t)$, which is the time-domain counterpart of $\widehat{Q}_\mathrm{n}(\omega)$, after a weighting on the mode spatial distribution $\psi(x)$. The presence of this random forcing represents an opportunity for the development of system identification methods. It "shakes" the system dynamics away from its deterministic trajectories, thus enriching the statistics of the output signals, allowing the system to visit states that it would never access if noise were not present.

2.2. Colored noise model

In a bounded system it is possible to extract, using methods such as the ones described in [12], the acoustic pressure generated by the heat release fluctuation source. It is however impossible

to measure the sources $\widehat{Q}_\mathrm{n}$ and $\widehat{Q}_\mathrm{a}$ and their respective emitted sounds independently. Tests like those presented in fig. 1 and fig. 2 are performed removing the combustor's walls and placing the open flame in an anechoic room, so that one can measure the field generated by the incoherent heat release fluctuation only, i.e. the combustion noise. Therefore, if a model for that stochastic forcing is needed, combustion noise measurements are the only source of information. As seen before, combustion noise features a specific spectrum. Typically, this has rising power from low frequencies to a maximum, following approximatively $P \propto f^2$, and then slowly decaying with an approximately constant law for higher frequency: $P \propto f^{-r}, 2 < r < 3.4$ - see for instance [3]. The peak frequency of the combustion noise spectrum can be estimated making use of experimental relations such as the one proposed in [13], involving dimensions, flow properties and chemical quantities. Alternatively, it has been observed [3] that, defining the Strouhal number as $St = f_\mathrm{max} L_\mathrm{F}/U_\mathrm{avg}$, where L_F is the flame length, this dimensionless group is almost in any case close to 1, hence $f_\mathrm{max} \approx U_\mathrm{avg}/L_\mathrm{F}$. This evidence is presented in the inset of fig. 2. The heat release fluctuation constituting the incoherent source term ($\widehat{Q}_\mathrm{n}$ in this work) have a low-pass characteristic, i.e. its spectrum is constant up to the cut-off frequency, and then it decays with the same power law of the combustion noise. The power spectrum S_{qq} of $\widehat{Q}_\mathrm{n}$ can be approximated with different analytical expressions, to obtain a model for the source term to be used in the remainder of this work. According to a mode-decomposition vision, more suitable in the context of bounded systems, $\widehat{Q}_\mathrm{n}$ is projected on the mode shape $\psi(x)$, obtaining after an inverse Fourier transform $\xi(t)$ (see eq. (1)). The essential feature of this stochastic forcing is its non-zero correlation or, equivalently, this is a colored noise. This fact, taking as reference a white noise, results into an additional parameter needed to describe it, i.e. its correlation time.

In literature one can find a wide collection of studies featuring colored noise, in topics ranging from electrical engineering to mathematics, from biology to mechanics. Some references for colored noise driven oscillators are [14] or [15]. [16] shows the effect of three different noises (white, blue and pink) on thermoacoustic dynamics in a context of limit-cycle triggering. In [17] a complete discussion about any $1/f^r$ noise generation for simulation purposes is addressed. In some works, such as [18], the Lorentzian, or *"quasi monochromatic"* noise is adopted. In most of the cases where the noise has low-pass characteristic, ξ is provided as the result of an Ornstein-Uhlenbeck process. In fact, this has a low-pass frequency spectrum, with a power decay $P \propto f^{-2}$ beyond the cut-off frequency, and an exponentially decaying autocorrelation. This model is an adequate representation of actual experimental data, as shown in fig. 1 (black line), where it matches the $\widehat{Q}_\mathrm{n}$ power spectrum spectrum S_{qq}.

From a mathematical point of view, ξ is the result of the differential equation:

$$\dot{\xi}(t) = -\frac{1}{\tau_\mathrm{c}}\xi(t) + \frac{\sqrt{\gamma}}{\tau_\mathrm{c}}\zeta(t), \tag{4}$$

where ζ is a unit-variance Gaussian white noise of intensity Γ, γ is a constant coefficient used later to adjust the power of the noise and τ_c is the noise characteristic time constant. Equivalently, ξ

can be obtained applying to ζ the filter H:

$$H(s) = \frac{\widehat{\xi}(s)}{\widehat{\zeta}(s)} = \frac{\sqrt{\gamma}}{1+\tau_c s}. \tag{5}$$

The resulting power spectrum of $\xi(t)$ is then given by $|H|^2 S_{\zeta\zeta}$:

$$S_{\xi\xi}(\omega) = \frac{\Gamma}{2\pi}\frac{\gamma}{1+\omega^2\tau_c^2}, \tag{6}$$

As discussed in the Introduction, if one wants to perform SI with a single mode description, then one has to focus the analysis in a band $[\omega_1;\omega_2]$ around one of the system's natural pulsations ω_0. The value of γ can be chosen to equate the powers provided by ξ and by a white noise of intensity Γ in that band ($\int_{\omega_1}^{\omega_2} S_{\xi\xi} d\omega = \int_{\omega_1}^{\omega_2} \Gamma/2\pi d\omega$), obtaining:

$$\gamma = \frac{\tau_c(\omega_2-\omega_1)}{\arctan(\omega_2\tau_c) - \arctan(\omega_1\tau_c)}. \tag{7}$$

τ_c is a direct measure of how "colored" the noise is: the shorter τ_c, the closer ξ is to a white noise. In agreement with that, in the limit $\tau_c \to 0$, one gets $\gamma \to 1$ and $S_{\xi\xi}(\omega) \to \Gamma/2\pi = S_{\zeta\zeta}(\omega)$.
The band $[\omega_1;\omega_2]$, which is henceforth referred as "iso-power band", can be expressed via the parameter $\Delta\omega$:

$$[\omega_1;\omega_2] = [\omega_0 - \Delta\omega; \omega_0 + \Delta\omega]. \tag{8}$$

$\Delta\omega$ (henceforth "iso-power semi-bandwidth") can vary between 0 (band degenerating in the single pulsation $\omega_0 = 2\pi f_0$) and ω_0 (band $[0; 2\omega_0]$). $\Delta\omega$ will play a fundamental role in the remainder of this work. One can see in fig. 5 how this parameter affects the noise power spectrum. Note that $S_{\xi\xi}(\omega_0) \neq \Gamma/2\pi$.
The characteristic time τ_c is the noise correlation time, as obtained via the autocorrelation function of ξ (inverse Fourier transform of its power spectrum),

$$k(t) = \Gamma\frac{\gamma}{2\tau_c}e^{-\frac{t}{\tau_c}}, \quad \tau_c = \frac{1}{k(0)}\int_0^\infty |k(t)|dt. \tag{9}$$

2.3. Colored noise driven Van der Pol oscillator

In order to estimate the effects of noise color on the dynamics of a thermoacoustic system, a simplified model consisting in two coupled van der pol oscillators is used. It contains a limited number of parameters, but it still represents well the dynamics observed in combustion chambers. A noise ξ is used to force the system, mimicking the non-coherent heat release fluctuations. ξ will be modeled either like a white noise or like a colored noise, in order to compare the response of the model, under different characteristic parameters. In fig. 6, MATLAB® and Simulink® simulation results for a system of two coupled VdP oscillators driven by colored noise are presented. The total pressure power spectrum is similar to the experimental one (compare with fig. 3), and clarifies what is hidden behind a single-mode approximation. The total output p is the sum of the outputs of

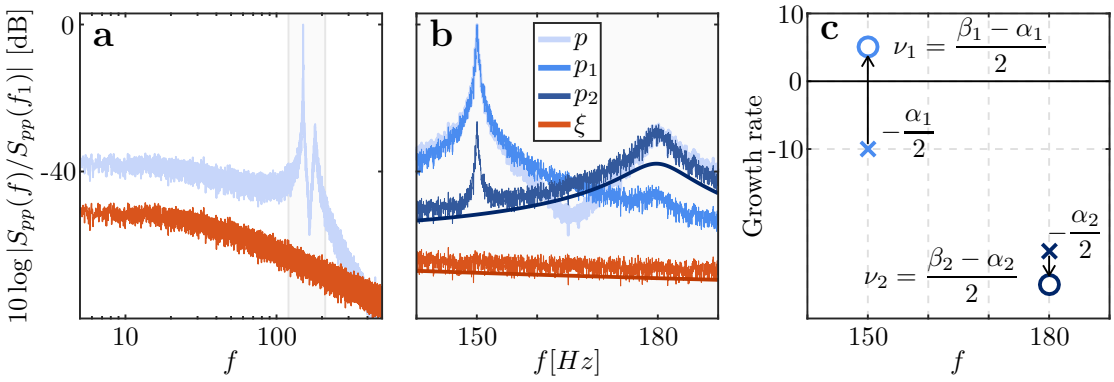

Figure 6: Double Van der Pol oscillator simulation results. The model is made of two VdP oscillators linearly coupled, and is fed by colored noise (eq. (6)). Oscillator #1 ($f_1 = 150$ Hz) is linearly unstable, oscillator #2 ($f_2 = 180$ Hz) is stable. a) Overview of the total pressure and forcing noise spectra. b) The spectral SPL of total pressure, single oscillators pressure p_1 and p_2, and forcing noise, in the frequency band that encloses the two oscillators' natural frequencies. c) The poles shift due to the feedback action, that can either destabilise or increase the stability margin of the mode.

the two oscillators p_1 and p_2. Note the difference (thin and thick dark blue lines) between the simulated and the theoretical spectrum of p_2. The main difference between the two is for $f = f_1$. This is because these oscillators are coupled and the linearly unstable oscillator #1, characterized by a limit-cycle at f_1, is forcing oscillator #2. At the same time, the linearly stable mode (oscillator #2) contributes to S_{pp} around the eigenfrequency $f_1 = 150$ Hz of the unstable mode (oscillator #1). Its effect is present directly at each frequency in the output of the system, as $p = p_1 + p_2$, and indirectly as it is part of the feedback action that forces both VdP oscillators. Therefore, it is not exact to state that the response of the system at $f = f_1$ is just due to the oscillator #1. However, if the two peaks are distant enough and one is stronger than the other, these contributions are negligible, compared to the direct output of the oscillator #1 at its natural frequency. Restricting the discussion to this case, one can adopt the aforementioned single-mode approximation.
If one single mode j dominates in the system, the pressure field can be then approximated by $p(x,t) = \eta_j(t)\psi_j(x)$, with η_j governed by:

$$\ddot{\eta}_j + \omega_j^2 \eta_j = f_j(\eta_j, \dot{\eta}_j) + \xi_j. \tag{10}$$

Assuming the damping of the system to be linear, one can write: $f_j(\eta_j, \dot{\eta}_j) = \dot{q}_\mathrm{a} - \alpha\dot{\eta}_j$, where α is the damping constant. $q_\mathrm{a}(t)$ is the inverse transform of $\widehat{Q}_\mathrm{a}(\omega)$, and it therefore represents in the time domain the heat release fluctuation coherent with the acoustic field. A common response of turbulent flames to acoustic excitation features a linear increase of heat release fluctuation for low forcing amplitude, followed by a saturation (see for example [19, 20]). For small and moderate amplitudes, this last aspect can often be approximated via a cubic term, therefore one can assume $q_\mathrm{a} = \beta\eta_j - \kappa\eta_j^3/3$ (see Appendix A for details). Considering that, one gets the Van der Pol (VdP)

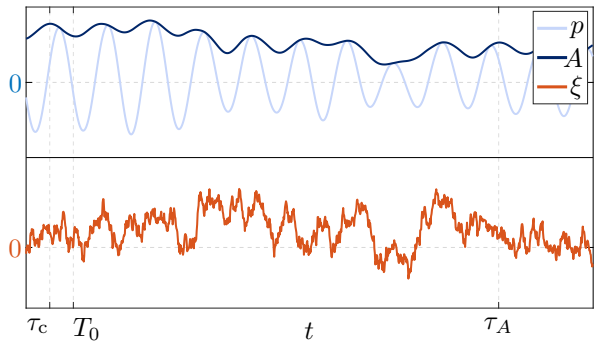

Figure 7: Time scales involved in a thermoacoustic system: τ_c correlation time of the source noise ξ, $T_0 = 1/f_0$ acoustic period of p, $\tau_A = 1/2|\nu|$ pressure amplitude A characteristic time scale [22].

oscillator's equation:

$$\ddot{\eta}_j + \omega_j^2 \eta_j = [2\nu - \kappa \eta_j^2]\dot{\eta}_j + \xi_j \tag{11}$$

where $\nu = (\beta - \alpha)/2$ is the linear growth rate.
It is convenient to recast this equation using the amplitude-phase coordinates. This substitution is legitimate as, in most of the practical cases, the thermoacoustic systems are in the class of "weakly" amplified/damped ones. This means that the right hand side of eq. (10) is much smaller than the left one and then $\eta(t) \approx A(t)\cos[\omega t + \varphi(t)] = A(t)\cos\phi(t)$. Following the derivation provided in Appendix A and using the model (6) for ξ, deterministic and stochastic averaging [21] yields the stochastic differential equation:

$$\dot{A} = A\left(\nu - \frac{\kappa}{8}A^2\right) + \frac{\Gamma}{4\omega_0^2 A}\frac{\gamma}{(1+\omega_0^2\tau_c^2)} + \mu, \tag{12}$$

where μ is another noise source resulting from the stochastic averaging.
Again, in the limit of $\tau_c \to 0$, eq. (12) reduces to its counterpart for a white noise driven system:

$$\dot{A} = A\left(\nu - \frac{\kappa}{8}A^2\right) + \frac{\Gamma}{4\omega_0^2 A} + \mu. \tag{13}$$

The averaging method is valid if the correlation times are such that $\tau_\xi \ll \tau_A$ [21]. This is generally verified for practical cases. The amplitude correlation time is related to the growth rate by $\tau_A \simeq 1/2|\nu|$ [22]. Taking, for example, $\nu = 10$ rad/s, $\tau_A = 50$ ms, while the noise correlation time $\tau_c \approx 1/2\pi f_{\max}$ is generally smaller than 1 ms ($f_{\max} \geq 50$ Hz, see fig. 2). These characteristic times are presented in fig. 7. Considering the Fokker-Planck equation (see [23]) associated with eq. (12) , one can derive the stationary probability distribution (PDF) for the amplitude of the colored noise driven VdP oscillator:

$$P_c(A) = \mathcal{N}_c A \exp\left[\frac{4\omega_0^2}{\Gamma}\frac{(1+\omega_0^2\tau_c^2)}{\gamma}\left(\frac{\nu A^2}{2} - \frac{\kappa A^4}{32}\right)\right], \tag{14}$$

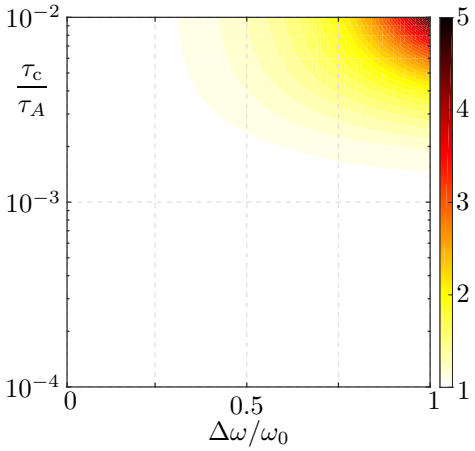

Figure 8: Map of the coefficient $(1+\omega_0^2\tau_c^2)/\gamma$. The closer this is to one, the closer the analytical expressions for P_c and P_w are.

and for the white noise driven VdP oscillator:

$$P_w(A) = \mathcal{N}_w A \exp\left[\frac{4\omega_0^2}{\Gamma}\left(\frac{\nu A^2}{2} - \frac{\kappa A^4}{32}\right)\right], \tag{15}$$

where $\mathcal{N}_c$ and $\mathcal{N}_w$ are two normalisation constants defined by $\int_0^\infty P(A)dA = 1$.
For a given set of system parameters (ν, κ, ω_0), $P_w(A)$ depends only on the white noise intensity Γ, whereas $P_c(A)$ is also function of the colored noise time scale τ_c and of the iso-power semi-bandwidth $\Delta\omega$ (through γ, defined in eq. (7)). Apart for the normalisation constants, P_c and P_w differs for the factor $(1+\omega_0^2\tau_c^2)/\gamma$ in the exponent. In fig. 8 one can see a map of its value, as function of the iso-power bandwidth $\Delta\omega$ and of the source noise correlation time τ_c. This is a first qualitative indication of the effect of the introduction of noise color in the model. For short τ_c and narrow $\Delta\omega$, this coefficient is close to one (white), meaning that the two analytical expressions for P_c and P_w are identical. For larger values of those two parameters, however, this coefficient increases (darker colors in the map). Accordingly, P_c and P_w can show significant differences, as depicted in fig. 9 and investigated in more detail in the next section.

3. Noise color in system identification methods

In this section, the white noise approximation is compared to the more realistic colored noise model, using as a meter the difference between the respective analytical expressions for the amplitude PDFs (eqs. (14) and (15)). The amplitude PDF is used with success for system identification purposes, and the discussion of this section is oriented in that sense.

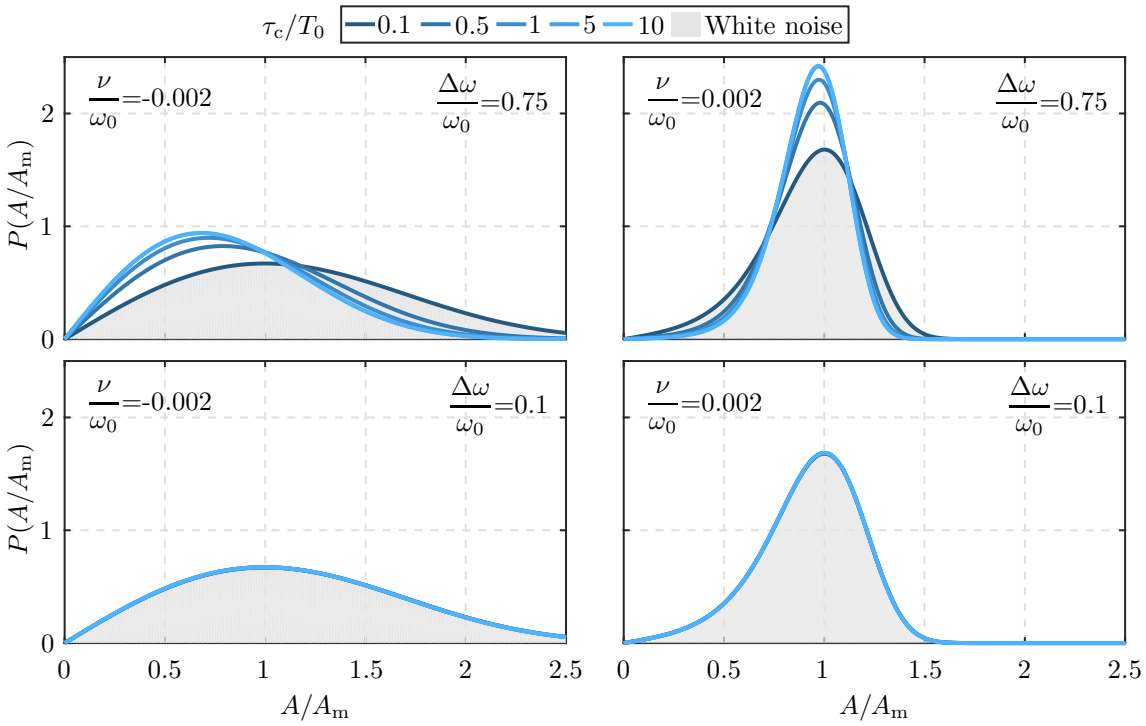

Figure 9: Probability density function for two different linear growth rates ν, two different iso-power semi-bandwidth $\Delta\omega$, and five different adimensional correlation times τ_c/T_0 of the driving noise (where $T_0 = 2\pi/\omega_0$ is the acoustic period). Solid lines are the PDFs for colored noise VdP (eq. (14)), shaded area the white noise driven PDF (eq. (15)) for the same parameters. The amplitude A is given as relative to A_m, the amplitude of the $P_w(A)$ maximum.

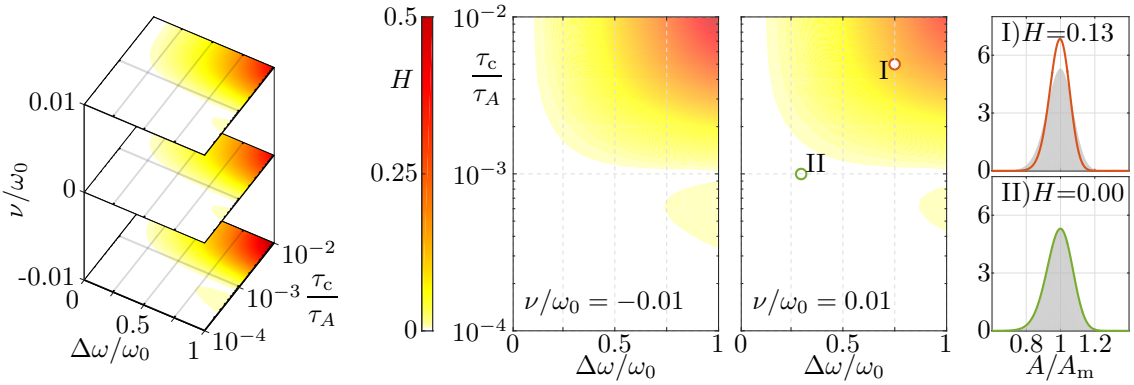

Figure 10: Hellinger distance (16), quantifying the difference between the PDFs of colored noise and white noise driven VDP oscillators. Left: different maps in the space $(\Delta\omega, \tau_c, \nu)$. Right: detail of a linearly stable and of a linearly unstable cases. The correlation time of the noise is normalised on the correlation time of the pressure amplitude $\tau_A = 1/2|\nu|$. The linear growth rate ν is normalised on the oscillators' pulsation ω_0.

This is a pre-print version. Presented at *International Symposium: Thermoacoustic Instabilities in Gas Turbines and Rocket Engines*, May 30 - June 02, 2016 Munich, Germany.

3.1. Colored vs white noise

The difference between the PDF of colored noise driven system P_c and the one obtained adopting the white noise approximation P_w is related to the reliability of all the methods that exploit the experimental PDF for identifying the system parameters. Indeed, if the two were significantly different, the white noise assumption would be brought into question.

Examples of the effect of noise power and correlation time influence on the PDF are given in Figure 9. The system parameters are the same for both the white noise and the colored noise driven oscillators. In the latter, the additional parameter of correlation time of the noise is included, with different possible values. The colored noise intensity is chosen to have the same power as the white noise, in a band around the oscillator natural pulsation $[\omega_0(1 \pm \Delta\omega)]$. In the four panels, one can see the analytical PDFs for two different values of the linear growth rate ν (columns) and two different iso-power band (rows). In the case of a wide iso-power band, one can observe a substantial difference for certain values of the correlation time. On the other hand, when the band is narrow, P_c matches well P_w, whatever the correlation time of the noise.

The growth rate parameter ν determines, with its sign, whether the system is linearly stable or not. If $\nu < 0$, the oscillator deterministic equilibrium amplitude is $A = 0$, but the presence of the noise results in a non-zero amplitude of maximum probability ($A_m > 0$). If $\nu > 0$, the amplitude of the limit cycle due to nonlinear saturation is $A_{det} = \sqrt{8\nu/\kappa}$. For any ν it can be observed that, compared to a white noise of the same power, the colored noise let the system stay closer to its deterministic amplitude. In fact, in the linearly stable case (left column), the amplitude of maximum probability is moved towards lower values of A (closer to the rest position), and the PDF becomes less spread. In the linearly unstable case (right), the amplitude of maximum probability A_m does not change, because is governed by ν itself and the saturation strength κ, but, again, a narrowing of the PDF is observed. This aspect could be linked to the correlation of noise. In fact, the white noise changes from instant to instant with no underlying trend. This gives no time to the system to adapt the response to the external forcing, resulting in a stronger distancing from the deterministic behaviour of the oscillator.

Note that in case of experimental data analysis the whole process is generally inverse. In fact, one tries to fit a theoretical "white noise PDF" P_w^{fit} on the experimental one (by nature "colored", P_c^{exp}), in order to identify the system parameters. When the effect of noise color is no more negligible, the P_w^{fit} that fits into P_c^{exp} has incorrect parameters, as the P_w with the right ones would be sensibly different. Therefore, if one knows the difference between the theoretical P_w and P_c for any combination of parameters, then is possible to check if the white noise approximation will yield a correct identification.

To obtain a quantitative measure of that difference, one can make use of the Hellinger distance:

$$H = \sqrt{1 - Bh}, \tag{16}$$

where $Bh = \int_{-\infty}^{+\infty} \sqrt{p(x)q(x)}dx$ is the Bhattacharyya coefficient. The Hellinger distance is a statistic quantity that measures the closeness of two PDFs of the same random variable $p(x)$ and

$q(x)$, and ranges from 0 ($p(x) = q(x)$) to 1 ($p(x)$ and $q(x)$ non-zero on different interval of x).
In this section, H is computed to compare $P_c(A)$ and $P_w(A)$ for different points $(\Delta\omega, \tau_c, \nu)$ of the space of iso-power bandwidth, correlation time and growth rate. The results are presented as a colormap in fig. 10. White regions correspond to values of H close to 0, i.e. where P_w is similar to P_c, while dark regions correspond to combinations of parameters that leads to a substantial difference between the two.
All the maps are similar, whatever the system's linear growth rate. The overwhelming majority of the area is light-colored, meaning that the white noise model matches the colored one for a wide range of parameters values. The two PDFs start to be different and the area to be dark in the upper-right corner of the map, i.e. for high values of $\Delta\omega$ and τ_c. All the three investigated parameters have an effect on the difference between P_c and P_w.
It can be observed that P_c and P_w are different for lower values of $\Delta\omega$ and τ_c when $\nu < 0$, meaning that the noise color has a slightly stronger effect. This is due to the shift of the amplitude of maximum probability A_m, observed in the linearly stable case for non-negligible values of τ_c.
The influence of τ_c is intrinsically related to the noise color: as discussed in section 2.2, the shorter τ_c, the closer is ξ to a white noise (which has $\tau_c = 0$). That is why the region of match between P_c and P_w ($H \approx 0$, white in the map) is wider for short correlation times.
$\Delta\omega$ has also a strong influence: for large bandwidth P_c and P_w are different. This has an impact on the choice of the filter bandwidth, if the experimental data need to be processed, and it is actually the only parameter on which one can play, given that the other two depends on the system properties. Given (τ_c, ν) and an accepted discrepancy between P_w and the more accurate P_c, the Hellinger map provides an indication on the maximum filter size to adopt, in order not to misinterpret the actual amplitude dynamics. It is however more likely to be able to guess a range of possible noise correlation times, rather than its exact value. This is possible, e.g. making use of empirical relations such as the one mentioned in section 2.2. The same can be argued for ν, although it plays a minor role for this specific issue. This fact prevent to use the Hellinger map in a systematic way, for computing the exact filter size to adopt. However, this result highlights the importance of focusing the analysis of experimental data on a limited band around the frequency of interest, when one attempt a single-mode SI using the amplitude PDF. In fact, even if the studied mode were completely isolated from the others, the error brought by the noise modelling would be significant, if one completely ignored its actual power spectrum and try to draw conclusions using the unfiltered pressure time trace or, equivalently, the complete acoustic pressure spectrum.
Nevertheless, for low values of τ_c (reasonable in actual combustion chambers), the map shows that the mismatch between P_w and P_c is not critical, as it is possible to adopt large iso-power bandwidth, with a semi-width up to the order of $0.5 f_0$. This allows one to state that the white noise approximation is satisfactory in most of the situations.
Therefore, summing up, the effect of noise color in thermoacoustic system is more significant for:

- driving noises featuring longer correlation times τ_c,

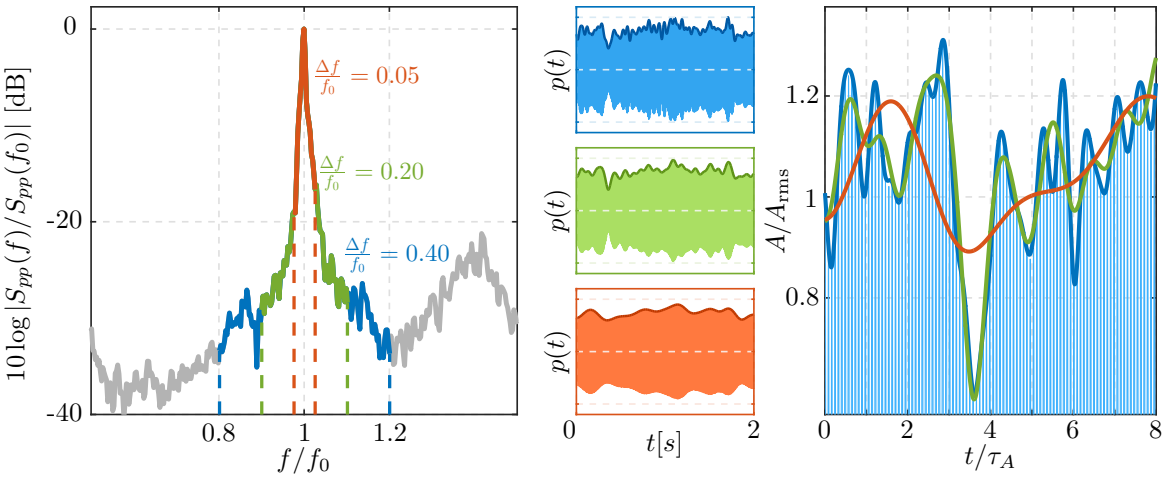

Figure 11: Effects of three different filter bandwidths on the analysis of combustor pressure experimental data. Left: acoustic pressure spectrum and filters bands. Center: time traces resulting from the three different filtering. Right: detail of the envelopes over eight τ_A.

- wider iso-power bandwidth $\Delta\omega$,

However,

- in most of the practical cases, for realistic values of ν and τ_c, and not adopting an extremely wide $\Delta\omega$, the white noise approximation is satisfactory.

In addition to that, actual spectra often feature sensible peaks around the main one. This, as discussed in the next section 3.2, is a further constraint when one analyses experimental data and performs SI.

3.2. Filter size for system identification

A typical combustor acoustic pressure spectrum features different peaks (fig. 3). As seen in the simulated double VDP oscillator (fig. 6), the different modes acting in the domain are mutually coupled, each one influencing the response of the others. However, if the neighbouring peaks of the spectrum are not too close, one can analyse one mode at a time, isolating its dynamic from that of the other modes. This can be easily done by bandpass filtering the data. This simplifies the system identification, since neither the parameters of the neighbour mode, nor the coupling coefficients have to be taken into account .

Figure 11 shows a typical situation and the effects of a different filter bandwidth. This experimental spectrum features a strong peak, corresponding to the dominant mode's eigenfrequency, surrounded by two others small peaks. In order to identify the mode's characteristic parameters with accuracy, removing the other modes effect, one has to filter the signal around the peak. The maximum

bandwidth is the one that discards neighbouring peaks while keeping the main peak and its tails ($\Delta f/f_0 = 0.40$ in this case). One could also choose narrower bands ($\Delta f/f_0 = 0.20$ or $\Delta f/f_0 = 0.05$ in this case), obtaining different resulting time signals. However, in the last case, one can observe a complete loss of the information contained in the original signal. Looking at the right panel of fig. 11, one can see that in the first case (green), the dynamics on time scales comparable to the amplitude correlation time $\tau_A = 1/2|\nu|$ is preserved: compared to the widest filter (blue), only high frequency oscillations are lost. This means that the PDF of A is essentially unaffected. In the second case (red filter), the resulting signal follows the general trend of the pressure oscillations, but the signal statistics are altered, and no reliable identification is possible.
Therefore, when one analyses experimental data around a frequency of interest, there exist, for the filter bandwidth:

- an upper limit, given by the distance to the neighbouring peaks,
- a lower limit, given by the need to not alter the amplitude statistics.

This constraint has to be satisfied in parallel with the one regarding the validity of the white noise approximation (section 3.1). However, in most of the practical cases, neighbouring peaks are close and the filter bandwidth narrow enough that the effect of noise color can be safely neglected.

4. Conclusion

In this work, the effects on thermoacoustic systems of the color of turbulence induced noise has been investigated. The white noise approximation, often adopted in the context of data analysis and system identification, has been critically compared to the Ornstein-Uhlenbeck noise model, closer to experimental data. If the correlation time of the noise τ_c is not negligible, or the response of the system is examined in wide bands, one can observe significant differences between the two models for the same system's parameters. This results in a sensibly different amplitude probability density function, causing the system identification methods to loose accuracy if a white noise model is used for the identification of the actual system. In that case, one would have to perform the system identification using the colored noise driven Van der Pol oscillator with 2 more paramteres to identify. The accuracy of the white noise approximation for any combination of examined bandwidth, correlation time and growth rate can be estimated making use of some indicators, such as the Hellinger distance. While τ_c is an unknown parameter of the particular thermoacoustic system, the analysed band is generally chosen during the post-processing of experimental data, therefore care must be taken in that choice. However, it is rather more common in practical cases to filter the experimental pressure signal around an eigenfrequency of interest, to get rid of the neighbouring dynamics and perform a more reliable system identification of the parameters relative to that mode only. As a result, the filter window size is already constrained by the proximity of neighbouring peaks, and one does not have to concern about the color of the real driving noise. Hence, the white noise approximation is satisfactory for most of the practical cases and convenient,

as one parameter less (τ_c) is needed to describe the system. On top of that, a lower bound for the filter window has also to be considered in order not to loose the signal statistics and dynamics and achieve an accurate identification.
Combining all the constraints, there exists a range of possible filter bandwidth to apply to experimental data, that has to be:

- not too wide, in order to avoid the influence of the color of noise or, more frequently, the effect of neighbouring peaks,
- not too narrow, in order to not remove the useful information contained in the signal.

Acknowledgement

This research is supported by the Swiss National Science Foundation under Grant 160579.

Appendices

A. Derivation of the amplitude equation

In this appendix, the amplitude equation for a cubic Van der Pol oscillator is derived. This is in the class of non-conservative, non-linear oscillators. It obeys the second order differential equation $\ddot{\eta} = f_0(\eta, \dot{\eta}, t)$. When f_0 is such that the oscillator is quasi-harmonic (resonable for a thermoacoustic system model), one can write the solution of that problem as:

$$\eta(t) \approx A(t)\cos\left[\omega_0 t + \varphi(t)\right] = A(t)\cos\phi(t), \tag{17}$$

where $A(t)$ is a term that modulates the amplitude of the quasi-sinusoidal oscillations, and $\varphi(t)$ their phase. These two quantities, although they may assume conspicuous values, are supposed to vary slowly or, equivalently, they are approximatively constant over an acoustic period $T_0 = 2\pi/\omega_0$. Therefore one can neglect their time derivative over that time scale and write:

$$A = \sqrt{\eta^2 + (\dot{\eta}/\omega_0)^2}, \tag{18a}$$

$$\varphi = -\arctan\left(\frac{\dot{\eta}}{\eta\omega_0}\right) - \omega_0 t. \tag{18b}$$

Deriving in time the latter two, and considering again eq. (10), one gets:

$$\dot{A} = -\frac{\sin\phi}{\omega_0} f(A\cos\phi, -A\omega_0\sin\phi) - \frac{\sin\phi}{\omega_0}\xi, \tag{19a}$$

$$\dot{\varphi} = -\frac{\cos\phi}{A\omega_0} f(A\cos\phi, -A\omega_0\sin\phi) - \frac{\cos\phi}{A\omega_0}\xi. \tag{19b}$$

This is a pre-print version. Presented at *International Symposium: Thermoacoustic Instabilities in Gas Turbines and Rocket Engines,* May 30 - June 02, 2016 Munich, Germany.

The function f can be expanded in Taylor series:

$$f(\eta, \dot{\eta}) = \sum_m \sum_n c_{m,n} \eta^m \dot{\eta}^n. \tag{20}$$

Then one can apply to the first right hand term of (19a) a deterministic averaging over one acoustic period and keep terms up to $\mathcal{O}(A^3)$, obtaining:

$$\dot{A}_{\mathrm{det}} = \frac{1}{2} c_{0,1} A + \left(\frac{1}{8} c_{2,1} + \frac{3\omega_0^2}{8} c_{0,3} \right) A^3. \tag{21}$$

The remaining term is stochastically averaged following the procedure proposed in [21]. The stochastic part of (19a) is recast making use of the rectangular coordinates $x = -\xi(t) \sin \phi(t)$ and $y = \xi(t) \cos \phi(t)$. As the correlation time of the noise is assumed to be much shorter then the characteristic time of A, one can find a time shift $\Delta \gg \tau_{\mathrm{c}}$, over which A and φ still do not change appreciably. One can then expand x in φ, around $\varphi(t - \Delta) = \varphi_{-\Delta}$:

$$x \approx -\xi(t) \sin(\omega_0 t + \varphi_{-\Delta}) - \xi(t) \cos(\omega_0 t + \varphi_{-\Delta}) \Delta\varphi. \tag{22}$$

Unlike $\varphi(t)$, $\varphi_{-\Delta}$ is stochastically independent from $\xi(t)$, so one can average the two separately:

$$\langle x \rangle = -\cos(\omega_0 t + \varphi_{-\Delta}) \langle \xi \Delta\varphi \rangle. \tag{23}$$

One can then integrate the fluctuating term of eq. (19b), obtain $\Delta\varphi$, and then express $\langle x \rangle$ as:

$$\langle x \rangle = -\frac{1}{\omega_0 A} \int_0^{\Delta} \langle \xi \xi_\tau \rangle \cos\phi \cos(\phi - \omega_0 \tau) d\tau. \tag{24}$$

For an Ornstein-Uhlenbeck noise, $\langle \xi \xi_\tau \rangle = \Gamma \dfrac{\gamma}{2\tau_{\mathrm{c}}} e^{-\tau/\tau_{\mathrm{c}}}$. This autocorrelation function goes quickly to zero for time larger than τ_{c}. Therefore, one can extend to infinity the upper limit of the integral in (24) and, keeping the non-oscillatory part only, get:

$$\langle x \rangle / \omega_0 = \dot{A}_{\mathrm{stoch}} = \frac{\Gamma}{4\omega_0^2 A} \frac{\gamma}{(1 + \omega_0^2 \tau_{\mathrm{c}}^2)}. \tag{25}$$

This term exists due to the correlation between $A(t)$ and $\varphi(t)$, which causes the fluctuating component to have a non-zero average.

One has then to consider $x' = x - \langle x \rangle$, a zero mean process constituted by all that is left from the stochastic averaging. Comparing with (22) and (23), one can approximate $x' \approx -\xi(t) \sin(\omega_0 t + \varphi_{-\Delta})$. Therefore, $\langle x' x'_\tau \rangle \approx \frac{1}{2} \langle \xi \xi_\tau \rangle \cos(\omega_0 t)$, so μ is, again, a colored noise.

In order to proceed, one has to provide an expression for $f(A \cos\phi, -A\omega_j \sin\phi)$. A common response of turbulent flames to acoustic excitation features a linear increase of heat release fluctuation for low forcing amplitude, followed by a saturation [19, 20]. For small and moderate amplitudes, this last aspect can be approximated via a cubic term:

$$q_{\mathrm{a}} = \beta\eta - \frac{\kappa}{3} \eta^3, \tag{26}$$

This is a pre-print version. Presented at *International Symposium: Thermoacoustic Instabilities in Gas Turbines and Rocket Engines,* May 30 - June 02, 2016 Munich, Germany.

where β and κ account for linear growth and nonlinear saturation. This yields:

$$f(\eta, \dot{\eta}) = \dot{\eta}(\beta - \alpha - \kappa\eta^2). \tag{27}$$

Comparing this to (20), substituting accordingly the constants $c_{m,n}$ in (21) and recollecting all the previous terms, one obtains eq. (12) and, in the limit $\tau_c \to 0$, (13).

References

[1] N. Noiray and B. Schuermans, "Deterministic quantities characterizing noise driven Hopf bifurcations in gas turbine combustors," *International Journal of Non-Linear Mechanics*, vol. 50, pp. 152–163, 2013.

[2] T. C. Lieuwen, *Unsteady combustor physics*. Cambridge University Press, 2012.

[3] R. Rajaram and T. Lieuwen, "Acoustic radiation from turbulent premixed flames," *Journal of Fluid Mechanics*, vol. 637, pp. 357–385, 2009.

[4] B. Schuermans, F. Guethe, D. Pennell, D. Guyot, and C. O. Paschereit, "Thermoacoustic modeling of a gas turbine using transfer functions measured under full engine pressure," *Journal of Engineering for Gas Turbines and Power*, vol. 132, no. 11, p. 111503, 2010.

[5] J. Li and A. S. Morgans, "Time domain simulations of nonlinear thermoacoustic behaviour in a simple combustor using a wave-based approach," *Journal of Sound and Vibration*, vol. 346, pp. 345–360, 2015.

[6] C. F. Silva, T. Emmert, S. Jaensch, and W. Polifke, "Numerical study on intrinsic thermoacoustic instability of a laminar premixed flame," *Combustion and Flame*, vol. 162, no. 9, pp. 3370–3378, 2015.

[7] G. A. Mensah and J. P. Moeck, "Efficient computation of thermoacoustic modes in annular combustion chambers based on bloch-wave theory," in *ASME Turbo Expo 2015: Turbine Technical Conference and Exposition*, American Society of Mechanical Engineers, 2015.

[8] T. C. Lieuwen, "Statistical characteristics of pressure oscillations in a premixed combustor," *Journal of Sound and Vibration*, vol. 260, pp. 3–17, 2003.

[9] F. Culick and P. Kuentzmann, "Unsteady motions in combustion chambers for propulsion systems," tech. rep., DTIC Document, 2006.

[10] W. Strahle, "Combustion noise," *Progress in Energy and Combustion Science*, vol. 4, pp. 157–176, 1978.

[11] C. Hirsch, J. Wäsle, A. Winkler, and T. Sattelmayer, "A spectral model for the sound pressure from turbulent premixed combustion," *Proceedings of the Combustion Institute*, vol. 31, no. 1, pp. 1435–1441, 2007.

[12] C. O. Paschereit, B. Schuermans, W. Polifke, and O. Mattson, "Measurement of transfer matrices and source terms of premixed flames," *Journal of Engineering for Gas Turbines and Power*, vol. 124, no. 2, pp. 239–247, 2002.

[13] B. Shivashankara, W. Strahle, and J. Handley, "Combustion noise radiation by open turbulent flames," *Progress in Astronautics and Aeronautics*, vol. 37, pp. 277–296, 1975.

[14] J. Masoliver and J. M. Porra, "Harmonic oscillators driven by colored noise: Crossovers, resonances, and spectra," *Physical Review E*, vol. 48, no. 6, p. 4309, 1993.

[15] Y. Xu, R. Gu, H. Zhang, W. Xu, and J. Duan, "Stochastic bifurcations in a bistable duffing–van der pol oscillator with colored noise," *Physical Review E*, vol. 83, no. 5, p. 056215, 2011.

This is a pre-print version. Presented at *International Symposium: Thermoacoustic Instabilities in Gas Turbines and Rocket Engines,* May 30 - June 02, 2016 Munich, Germany.

[16] I. Waugh, M. Geuß, and M. Juniper, "Triggering, bypass transition and the effect of noise on a linearly stable thermoacoustic system," *Proceedings of the Combustion Institute*, vol. 33, no. 2, pp. 2945–2952, 2011.
[17] N. J. Kasdin, "Discrete simulation of colored noise and stochastic processes and $1/f^{\alpha}$ power law noise generation," *Proceedings of the IEEE*, vol. 83, no. 5, pp. 802–827, 1995.
[18] W. Zhang, J. Casademunt, and J. Viñals, "Study of the parametric oscillator driven by narrow-band noise to model the response of a fluid surface to time-dependent accelerations," *Physics of Fluids A: Fluid Dynamics (1989-1993)*, vol. 5, no. 12, pp. 3147–3161, 1993.
[19] R. Balachandran, B. Ayoola, C. Kaminski, A. Dowling, and E. Mastorakos, "Experimental investigation of the nonlinear response of turbulent premixed flames to imposed inlet velocity oscillations," *Combustion and Flame*, vol. 143, no. 1, pp. 37–55, 2005.
[20] S. K. Thumuluru and T. Lieuwen, "Characterization of acoustically forced swirl flame dynamics," *Proceedings of the Combustion Institute*, vol. 32, no. 2, pp. 2893–2900, 2009.
[21] R. L. Stratonovich, *Topics in the theory of random noise*, vol. 2. CRC Press, 1967.
[22] N. Noiray, "Linear growth rate estimation from dynamics and statistics of acoustic signal envelope in turbulent combustors," *To be published*, 2016.
[23] C. W. Gardiner *et al.*, *Handbook of stochastic methods*, vol. 3. Springer Berlin, 1985.

This is a pre-print version. Presented at *International Symposium: Thermoacoustic Instabilities in Gas Turbines and Rocket Engines,* May 30 - June 02, 2016 Munich, Germany.